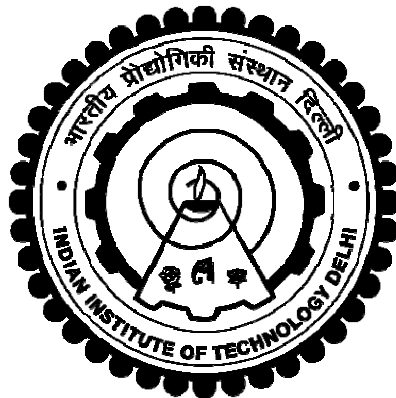


**EXPERIMENTAL AND NUMERICAL CHARACTERIZATION
OF GAS-LIQUID & GAS-LIQUID-SOLID FLOWS IN A
BUBBLE COLUMN/ SLURRY BUBBLE COLUMN**

PARUL TYAGI



**DEPARTMENT OF CHEMICAL ENGINEERING
INDIAN INSTITUTE OF TECHNOLOGY DELHI**

JULY 2017

©Indian Institute of Technology Delhi (IITD), New Delhi, 2017

**EXPERIMENTAL AND NUMERICAL CHARACTERIZATION
OF GAS-LIQUID & GAS-LIQUID-SOLID FLOWS IN A
BUBBLE COLUMN/ SLURRY BUBBLE COLUMN**

by

PARUL TYAGI

DEPARTMENT OF CHEMICAL ENGINEERING

submitted

in fulfillment of the requirements of the Degree of Doctor of Philosophy

to the



INDIAN INSTITUTE OF TECHNOLOGY DELHI

JULY 2017

“Dedicated to my parents, sister and almighty God”

Certificate

This is to certify that the thesis entitled “**Experimental and Numerical Characterization of Gas-Liquid and Gas-Liquid-Solid Flows in a Bubble Column/ Slurry Bubble Column**” being submitted by **Mrs. Parul Tyagi** for the award of the degree of **Doctor of Philosophy** in Chemical Engineering is a record of bonafide work carried out by her under my guidance and supervision at the Indian Institute of Technology Delhi. The results contained in the thesis have not been submitted elsewhere, either in part or full, to any other University or Institute for the award of any degree or diploma. I certify that she has pursued the prescribed course of research.

Dr. Vivek V. Buwa

Professor

(Supervisor of Student)

Department of Chemical Engineering

Indian Institute of Technology Delhi

Hauz Khas, New Delhi – 110016

Acknowledgments

Foremost, I would like to express my deepest gratitude to my supervisor **Prof. Dr. Vivek V. Buwa** for his guidance and encouragement during my doctoral study. I would like to thank him for giving my research an initial direction and always leaving me with his useful ideas and knowledge. His positive and timely feedback on my reports and presentations makes me to better focus on the main objectives of my research work.

I would like to thank the members of my research committee, **Prof. Dr. Ratan Mohan** and **Prof. Dr. Kamal K. Pant** and **Prof. Dr. Prabal Talukdaar** for investing their valuable time in examining my research work and providing me with some useful comments. I owe my invariably special thanks to **Prof. Dr. Ashok K. Gupta** for providing the fundamental knowledge of the core subjects and some important spiritual tips for the betterment of my life in IIT Delhi.

I would like to express my gratitude to the **Head of the Department of Chemical Engineering** for providing help for numerous academic formalities during my doctoral program. My thanks to the entire **Chemical Engineering Department** and secretaries for their help in making my work and life at IIT Delhi an enjoyable experience. I am grateful to the **IRD (IIT Delhi)** and **Human Resource Development Group (CSIR)** for the financial support to accomplish the research work. My research was carried out with the reliable and powerful framework for the simulations **Fluent, Ansys Inc.**. I

would like to thank Fluent support team for providing their help on various issues with user-defined routines. I warmly thank **Mr. Manish Agarwal** from Computer Service Center at IIT Delhi for his valuable support to access **HPC Cuda Cluster** facility to perform parallel processing of many simulations. I am also thankful to many people from the **Central Workshop, IIT Delhi** for the machining and fabrication of different devices and accessories. I thank **Mr. Anil** for his assistance during my experimental work.

My doctoral study would not have been so enjoyable without my lab colleagues **Ekta, Arpit, Sayanthani, Saroj, Abdul, Abhijeet, Sirisha** and **Brajesh** and my first lab colleagues, **Dr. Swapna Rabha** and **Dr. V. M. Rajesh**. My thank goes to many previous M.Tech. and B.Tech. students being involved in the projects related to my research area. I am thankful to my colleagues **Ekta Jain** and **Sirisha** for their generous help and support during the thesis-writing phase. I also thank my friends, **Usha, Meenakshi, Indu, Neerja, Shivani** and **Soniya** for many pleasant memories during my stay at IIT Delhi.

Last but not the least, my heartfelt gratitude goes to **my parents** for their endless love and continuous encouragement. I want to thank my elder sister **Mrs. Pooja Tyagi** for her constant support and for taking care of our parents. I thank all of them for always sharing many ups and downs in these years.

Above all, I thank the **Almighty God** for providing me knowledge and health with patience to withstand work pressure.

– Parul Tyagi

Abstract

Gas-liquid and gas-liquid-solid flows under the dilute flow conditions have been investigated widely, the characterization of such multiphase flows under dense flow conditions, i.e., at higher gas velocity and solid loading, remains to be difficult due to the complex flow behavior and phase interactions. Such dense multiphase flows in bubble column/ slurry bubble column offer challenges not only in their experimental characterization, but also in the development of computational models capable of predicting the dynamic and time-averaged flow characteristics. This research work is focused on characterization of dynamics of gas-liquid and gas-liquid-solid flows using the measurements of instantaneous and time-averaged flow characteristics, under dilute–to –dense flow conditions, and to develop experimentally verified computational models to predict the dynamics and time-averaged flow characteristics of gas-liquid and gas-liquid-solid flows in a bubble column/ slurry bubble column.

The first part of the present research work was devoted to understand the effect of poly-dispersity of bubbles on dynamics and time-averaged flow behavior of dispersed gas-liquid flow under dilute flow conditions ($\alpha_G < 10\%$). Measurements of instantaneous and time-averaged gas volume fraction, bubble size and rise velocity distribution were performed in a rectangular bubble column (with local needle sparger) using “in-house” developed voidage probes and high-speed camera. The dynamics of dispersed

gas-liquid flow with different bubble sizes ($d_B = \sim 0.1, 0.5, 1.0$ cm) was analyzed using instantaneous and time-averaged α_G , plume oscillation period and bubble rise velocity distribution at U_G in the range of 0.16 - 0.73 $cm.s^{-1}$. Simulations of the dilute gas-liquid flows were performed using Euler-Lagrange approach. The effect of size-dependent drag and lift forces on dynamic and time-averaged flow characteristics was investigated. The numerical predictions were verified using experimental measurements.

The other part of the research work was to develop experimentally verified Euler-Euler models to predict the dynamics and time-averaged flow behavior of the gas-liquid and gas-liquid-solid flow in a bubble column/ slurry bubble column under the dense flow conditions at high superficial gas velocities ($U_G > 5$ $cm.s^{-1}$) and or high solid loading ($\langle \alpha_S \rangle > 10$ vol.%). Measurements of overall and time-averaged α_G and its instantaneous fluctuations and bubble size distribution were performed in a rectangular column filled with a gas-liquid (air/water) and gas-liquid-solid (air/water/glass particles) system. The detailed investigations are performed to understand the effect of U_G and $\langle \alpha_S \rangle$ on the instantaneous α_G fluctuations arising due to column-scale and bubble-scale oscillations. Importantly, spatial-evolution of bubble size distribution and internal composition of gas volume fraction contained in different bubble size groups are presented.

Further, the two-/three-fluid Eulerian models were used to simulate the dense gas-liquid/ gas-liquid-solid flows in a pseudo 2D rectangle bubble column. The effect of U_G (up to 30 $cm.s^{-1}$) and $\langle \alpha_S \rangle$ (up to 40 vol.%) on the dynamic and time-averaged flow characteristics as numerically investigated. The simulation results were experimentally validated using measured instantaneous α_G time histories, frequency distribution and time-averaged gas volume fraction ($\bar{\alpha}_G$) profiles. A quantitative comparison of the dy-

dynamic characteristics inferred through instantaneous α_G time series and corresponding frequency analysis obtained using experiments and simulations showed a satisfactory agreement for the low-frequency oscillations arising due to meandering bubble plume.

A new set of experimental data on time-evolution of gas volume fraction, spatial-evolution of bubble size distribution and gas volume fraction contained in different bubble size groups, is suitable for the validation of multi-fluid CFD models coupled with populations balance model. The present work helps to improve the understanding of dynamics of dense-dispersed gas-liquid and gas-liquid-solid flows that will aid the development and verification of computational models for their numerical simulations.

सार

गैस-द्रव और गैस-द्रव-ठोस प्रवाह की जांच सरल प्रवाह की स्थिति के तहत व्यापक रूप से की गई है, परन्तु इस तरह के मल्टीफेज प्रवाह के व्यवहार का घने प्रवाह की स्थिति में, अर्थात्, उच्च गैस वेग और ठोस लोडिंग पर जटिल प्रवाह एवं फ़ेज के कारण लक्षण वर्णन करना मुश्किल हो जाता है। ऐसे घने मल्टीफेज प्रवाह का बबल कॉलम/ स्लरी बबल कॉलम में प्रवाह, न केवल उनके प्रायोगात्मक लक्षण वर्णन में चुनौतियां हैं, बल्कि उनकी तात्कालिक और समय-औसत प्रवाह की विशेषताओं की भविष्यवाणी करने में सक्षम कम्प्यूटेशनल मॉडल के विकास में भी चुनौतियां हैं। यह शोध कार्य, गैस-द्रव और गैस-द्रव-ठोस प्रवाह की गतिशीलता को तात्कालिक और समय-औसत प्रवाह विशेषताओं के माप का उपयोग करके सरल-से-घने प्रवाह की स्थिति के तहत बबल कॉलम/ स्लरी बबल कॉलम में गैस-तरल और गैस-तरल-ठोस प्रवाह की गतिशीलता और समय-औसत प्रवाह विशेषताओं अनुमान लगाने के लिए प्रयोगात्मक रूप से सत्यापित कम्प्यूटेशनल मॉडल विकसित करने पर केंद्रित है।

वर्तमान अनुसंधान कार्य का पहला भाग के गैस-द्रव के तात्कालिक और समय-औसत प्रवाह के व्यवहार पर, सरल प्रवाह की स्थिति (गैस मात्रा $< 10\%$) के तहत, बुलबुले की पाली-डिस्पेर्सिटी के प्रभाव को बबल कॉलम में समझने के लिए समर्पित था। तात्कालिक और समय-औसत गैस मात्रा के अंश, बुलबुला आकार और वेग वितरण को आयताकार बबल कॉलम (स्थानीय सुई स्पर्गर के साथ) में " इन-हाउस" विकसित वॉइडज सेंसर और हाई स्पीड कैमरा का उपयोग करते हुए मापा गया। गैस-द्रव प्रवाह का विभिन्न बबल आकार के साथ (बबल व्यास = 0.1, 0.5, 1.0 से.मी.) की गतिशीलता का तात्कालिक और समय-औसत गैस मात्रा, प्लूम दोलन अवधि और बबल वेग वितरण का उपयोग कर 0.16 - 0.73 से.मी./से. की सीमा के गैस वेग पर विश्लेषण किया गया। सरल गैस-द्रव प्रवाह के अनुमान लगाने के लिए सिमुलेशन यूजर-लाग्रांज का उपयोग किया गया। बबल आकार-निर्भर ड्रैग और लिफ्ट बलों के प्रभाव की जांच गति-आधारित और समय-औसत प्रवाह की विशेषताओं पर की गई। संख्यात्मक पूर्वानुमान प्रयोगात्मक मापों का उपयोग करते हुए सत्यापित की गई।

प्रयोगात्मक रूप से सत्यापित यूजर-यूजर मॉडल विकसित करना अनुसंधान कार्य का दूसरा भाग था ताकि एक बबल कॉलम/ स्लरी बबल कॉलम में गैस-द्रव और गैस-द्रव-ठोस प्रवाह के गतिशीलता और समय-औसत प्रवाह व्यवहार का घने प्रवाह की स्थिति में, अर्थात्, उच्च गैस वेग (गैस वेग > 5 से.मी./स.) और/या उच्च ठोस लोडिंग (> 10 वॉल्यूम %) के तहत अनुमान लगाया जा सके। तात्कालिक उतार-चढ़ाव और समय और समय-औसत गैस मात्रा, विभिन्न बुलबुले आकार समूहों के आधार पर गैस मात्रा का आंतरिक वितरण और बुलबुले के आकार वितरण की माप गैस-द्रव (वायु/ पानी) और गैस-द्रव-ठोस (हवा/ पानी/ कांच के कण) से भरे एक आयताकार बबल कॉलम में की गई। कॉलम-स्केल और बबल-स्केल दोलनों के कारण उत्पन्न गैस मात्रा में उतार-चढ़ाव पर गैस वेग और ठोस लोडिंग के प्रभाव को समझने के लिए विस्तृत जांच की गई। महत्वपूर्ण रूप से, बुलबुला आकार वितरण के स्थानिक-विकास और गैस के विभिन्न प्रकार के बुलबुले के आकार के समूहों में निहित आंतरिक मात्रा का वितरण प्रस्तुत किया गया है।

इसके अलावा, दो-/तीन-तरल यूलेरियन मॉडल का इस्तेमाल छद्म 2D आयताकार बबल कॉलम में घने गैस-द्रव और गैस-द्रव-ठोस प्रवाह को सिमुलेट करने के लिए किया गया। गैस वेग का प्रभाव (30 से.मी./स.) और ठोस लोडिंग (> 40 वॉल्यूम %) के प्रभाव की गतिशील और समय-औसत प्रवाह की विशेषताओं पर संख्यात्मक रूप से जांच की गई। सिमुलेशन के परिणाम प्रयोगात्मक रूप से मापे गए गैस मात्रा का समय श्रृंखला, आवृत्ति वितरण और समय औसत गैस मात्रा-प्रोफाइल का उपयोग करते हुए सत्यापित किये गए। प्रयोगों और सिमुलेशन से प्राप्त तात्कालिक गैस मात्रा अंश समय श्रृंखला और संबंधित आवृत्ति विश्लेषण के माध्यम से अनुमानित गतिशील विशेषताओं की एक मात्रात्मक तुलना कम-आवृत्ति बबल-प्लूम के कारण उत्पन्न होने वाले कम आवृत्ति दोलनों के लिए एक संतोषजनक समझौता देखा गया।

गैस मात्रा के समय-विकास, बबल आकार के वितरण के स्थानिक-विकास और बबल के आकार के समूहों में निहित गैस के मात्रा पर आधारित प्रयोगिक डेटा का एक नया सेट पापुलेशन-बैलेंस मॉडल के साथ मल्टी-फ्लूइड सीएफडी मॉडल की मान्यता के लिए उपयुक्त है। वर्तमान कार्य घने गैस-द्रव और गैस-द्रव-ठोस प्रवाह की गतिशीलता की समझ को बेहतर बनाने में मदद करता है जो कि उनकी संख्यात्मक सिमुलेशन के लिए कम्प्यूटेशनल मॉडल के विकास और सत्यापन में सहायता करेगा।

Table of Contents

Certificate	ii
Acknowledgments	iii
Abstract	v
Table of Contents	viii
Nomenclature	xii
List of Figures	xvi
List of Tables	xxx
Chapter 1 Introduction	1
1.1 Introduction	2
1.2 Motivation of the present research work	7
1.3 Key objectives	9
1.4 Organization of thesis	10
Chapter 2 Experimental Investigations of Gas-Liquid Flow	13
2.1 Present state of art	14
2.2 Experiments	18
2.2.1 Set-up for dilute gas-liquid flow experiments	18
2.2.2 Set-up for dense gas-liquid flow experiments	20
2.3 Measurement techniques	21

2.3.1	Development of voidage probes and signal processing	21
2.3.2	High-speed imaging and image processing	27
2.4	Experimental investigations of dilute gas–liquid flow	29
2.4.1	Results and discussions	29
2.4.2	Conclusions	43
2.5	Experimental investigations of dense gas–liquid flow	44
2.5.1	Results and discussion	44
2.5.2	Conclusions	64
Chapter 3	Experimental Investigations of Gas-Liquid-Solid Flow	66
3.1	Present state of art	67
3.2	Experiments	73
3.2.1	Experimental set-up	73
3.3	Results and discussion	76
3.3.1	Dynamics of dense gas-liquid-solid flow	76
3.3.2	Effect of solid loading on bubble size distribution	88
3.3.3	Effect of solid loading on time-averaged gas volume fraction distribution and its composition	93
3.4	Conclusions	99
Chapter 4	Euler-Lagrange Simulations of Dilute Gas-Liquid Flow	102
4.1	Present state of art	103
4.2	Computational model	106
4.2.1	Governing equations	106
4.2.2	Solution domain and boundary conditions	112
4.3	Results and discussion	114

4.3.1	Preliminary investigations	114
4.3.2	Dynamic flow characteristics	118
4.3.3	Time-averaged flow characteristics	126
4.3.4	Poly-dispersed gas-liquid flows: effect of size-dependent drag and lift force	132
4.4	Summary and conclusions	134
Chapter 5 Euler-Euler Simulations of Dense Gas-Liquid Flow		136
5.1	Present state of art	137
5.2	Computational approach and numerical background	140
5.2.1	Governing equations	140
5.2.2	Solution domain and boundary conditions	144
5.2.3	Modeling parameters	144
5.3	Results and discussion	147
5.3.1	Preliminary simulations	147
5.3.2	Dynamic flow behavior	154
5.3.3	Time-averaged flow behavior	160
5.4	Summary and conclusions	164
Chapter 6 Euler-Euler Simulations of Gas-Liquid-Solid Flow		167
6.1	Present state of art	168
6.2	Computational model and numerical schemes	170
6.2.1	Governing equations	171
6.2.2	Simulation procedure	176
6.3	Results and Discussions	179
6.3.1	Instantaneous flow behavior	179

6.3.2	Instantaneous gas phase characteristics	181
6.3.3	Overall gas volume fraction: experiments vs. three-fluid simu- lations	189
6.3.4	Spatial distribution of time-averaged gas volume fraction	190
6.4	Summary and conclusion	195
Chapter 7 Summary, Conclusions and Recommendations for Future Work		199
7.1	Summary	199
7.2	Key conclusions	202
7.2.1	Experimental Investigations	202
7.2.2	Numerical Investigations	204
7.3	Recommendations	207
Bibliography		208
List of Publications		234
Curriculum Vitae		236

Nomenclature

Symbols

C_1, C_2, C_μ	model constants in Eq. (5.6) and (6.13)
C_D	drag coefficient of bubbles swarm, -
C_{D_0}	drag coefficient for a bubble with constant d_B , -
C_L	lift coefficient, -
d	distance between the tips of a dual-tip probe, cm
d_B	bubble diameter, cm
D	column depth, cm
Eo	Eotvos number ($= g\Delta\rho d_B^2/\sigma$), -
f_s	sampling frequency, Hz
\vec{F}_D	drag force on a bubble, $kg.m^{-2}.s^{-2}$
\vec{F}_L	lift force on a bubble, $kg.m^{-2}.s^{-2}$
g	gradient vector in Eq. (2.13)
\vec{g}	gravitational acceleration, $m.s^{-2}$
G	turbulent generation due to mean velocity gradients
G_b	extra turbulent generation due to the presence of dispersed phase

G_i	Hessian matrix in Eq. (2.14)
H	column height, cm
H_D	dispersed liquid height, cm
k, K	raw moment
k	turbulent kinetic energy
m_B	mass of a bubble, kg
\vec{M}_{LG}	interphase momentum exchange between gas and liquid
N	total number of bubbles, -
P	pressure, Pa
P_S	solid pressure, Pa
P(R)	probability distribution function of the bubble radius, -
Q	Potential function in Eq. (2.15)
R	bubble radius, cm
Re_B	Reynolds number for bubble phase ($=\rho_L d_B (u_B - u_L) / \mu_L$), -
s	shape factor of a bubble, -
t	time, s
t_i	time required for passage of a bubble over a probe tip, s
Δt_E	Eulerian time-step, s
Δt_L	Lagrangian time-step, s
T	total sampling time, s

\vec{u}_B	bubble velocity, $m.s^{-1}$
\vec{u}_L	liquid velocity, $m.s^{-1}$
\vec{U}_L	mean liquid velocity, $m.s^{-1}$
U_G	superficial velocity, $cm.s^{-1}$
W	column width, cm
y	bubble chord length, cm
X, Y, Z	Cartesian coordinates

Greek letters

α_G	instantaneous gas volume fraction, -
$\overline{\alpha_G}$	time-averaged gas volume fraction, -
$\langle \alpha_S \rangle$	solid volume fraction, -
μ	molecular viscosity, Pa.s
ρ	density, $kg.m^{-3}$
Δ	interval variation of the random variable in Eq. (2.9)
λ	Lagrange multiplier, -
σ	variance in Eq. (2.20)
ε	turbulent energy dissipation rate
τ	characteristic time scale, s
$\overline{\overline{\tau_c}}$	viscous stress tensor
θ	granular temperature for solid particle, $m^2.s^{-2}$

Subscripts and superscripts

B	bubble
coll	collision
eff	effective
G	gas phase
i	counter
k, K	raw moment
kin	kinetic energy
L	liquid phase
LG	liquid to gas
S	solid phase
SL	solid to liquid
turb	turbulence

Abbreviations

BCR	bubble column reactor
CLD	chord length distribution
CFD	computational fluid dynamics
NT	noise removal threshold
PBM	population balance model
PDT	phase discrimination threshold
PSD	power spectral density
SBCR	slurry bubble column reactor

List of Figures

1.1	(a) Schematic of the local recirculatory flow structure in a three-dimensional cylindrical bubble column observed by Chen et al. (1994) and (b) different flow processes observed by Tzeng et al. (1993) in two-dimensional bubble column.	3
1.2	(a) Typical snapshots of (i) instantaneous and (ii) time-averaged liquid velocity distribution and (b) mixing time in a rectangular bubble column simulated by Buwa and Ranade (2003).	4
2.1	(a) Photograph of laboratory-scale rectangular bubble column and (b) typical needle sparger with 8 holes fixed in a 2.4 cm×1.2 cm area. . . .	19
2.2	(a) Laboratory-scale rectangular bubble column and (b) photograph of the in-house developed dual-tip voidage probe.	20
2.3	(a) typical voltage signal acquired by a dual-tip probe, (b) normalized phase discriminated signal and (c) typical distribution of number of gas points and corresponding time intervals that a probe tip spent in each bubble.	23

2.4	(a) Schematic of high-speed camera,(b) original photographs captured by high-speed camera and (c) binary images of captured photographs (also indicating bubble tracking in successive frames).	28
2.5	Snapshots of meandering motion of mono-dispersed ($d_B = \sim 0.5$ cm) bubble flow in a rectangular bubble column, (a) $U_G = 0.16$ $cm.s^{-1}$ and (b) $U_G = 0.73$ $cm.s^{-1}$ at different time intervals (i) t_0 , (ii) $t_0+2.0s$, (iii) $t_0+4.0s$, (iv) $t_0+6.0s$, (v) $t_0+8.0s$	30
2.6	Snapshots of meandering motion of mono-dispersed bubble flow, (a) $d_B = \sim 0.1$ cm at $U_G = 0.16$ $cm.s^{-1}$ and (b) $d_B = \sim 1.0$ cm at $U_G = 0.73$ $cm.s^{-1}$ at two different time instants.	31
2.7	Instantaneous α_G fluctuations recorded at different time-scales (τ) in mono-dispersed bubble flow ($d_B = \sim 0.5$ cm) at U_G of (a) 0.16 and (b) 0.73 $cm.s^{-1}$ (X = 10 cm, Y = 26.6 cm, Z = 2.5 cm).	32
2.8	Time-evolution of instantaneous α_G for mono-dispersed bubble flow ($d_B = \sim 0.5$ cm) at U_G of 0.16 and 0.73 $cm.s^{-1}$ at the liquid heights of (a) Y = 26.6 cm and (b) Y = 76.8 cm ($\tau = 0.5$ s, X = 10 cm, Z = 2.5 cm).	34
2.9	Power spectra corresponding to the α_G time series at (a) $U_G = 0.16$ $cm.s^{-1}$ and (b) $U_G = 0.73$ $cm.s^{-1}$ ($\tau = 0.5$ s, X = 10 cm, Y = 76.8 cm, Z = 2.5 cm).	35
2.10	Time-evolution of instantaneous α_G corresponding to the flow of mono-dispersed bubbles of rising different bubbles ($d_B = \sim 0.1, 0.5$ and 1.0 cm) at $U_G = 0.73$ $cm.s^{-1}$ ($\tau = 0.5$ s, X = 10 cm, Y = 56.7 cm, Z = 2.5 cm).	36

2.11	Power spectra corresponding to the flow of mono-dispersed bubbles, d_B = (i) ~ 0.1 cm, (ii) ~ 0.5 cm and (iii) ~ 1.0 cm at $U_G = 0.73 \text{ cm.s}^{-1}$ (τ = 0.5 s, $X = 10$ cm, $Y = 56.7$ cm, $Z = 2.5$ cm).	37
2.12	Photographs of mono-dispersed bubble flow of rising different bubble sizes injecting using different needle sizes (a) spherical bubbles, (b) ellipsoid bubbles and (c) wobbling bubbles.	38
2.13	Bubble size distribution for mono-dispersed bubble flow ($d_B = \sim 0.5$ cm) at (a) $U_G = 0.16 \text{ cm.s}^{-1}$ and (b) $U_G = 0.73 \text{ cm.s}^{-1}$	39
2.14	Bubble size distribution for mono-dispersed bubble flow (a) $d_B = \sim 0.1$ cm at $U_G = 0.16 \text{ cm.s}^{-1}$ and (b) $d_B = \sim 1.0$ cm at $U_G = 0.73 \text{ cm.s}^{-1}$	39
2.15	Bubble rise velocity distribution for mono-dispersed bubble flow ($d_B =$ ~ 0.5 cm) at (a) $U_G = 0.16 \text{ cm.s}^{-1}$ and (b) $U_G = 0.73 \text{ cm.s}^{-1}$	40
2.16	Bubble rise velocity distribution for mono-dispersed bubble flow (a) d_B = ~ 0.1 cm at $U_G = 0.16 \text{ cm.s}^{-1}$ and (b) $d_B = \sim 1.0$ cm at $U_G = 0.73$ cm.s^{-1}	40
2.17	Lateral distribution of time-averaged gas volume fraction for mono- dispersed bubble flow ($d_B = \sim 0.5$ cm) at different liquid heights (Y = 26.6 to 76.8 cm) for (a) $U_G = 0.16 \text{ cm.s}^{-1}$ and (b) $U_G = 0.73 \text{ cm.s}^{-1}$ ($Z = 2.5$ cm).	42
2.18	(a) Snapshots of dense gas-liquid flow in a rectangular bubble column and (b) local flow structure for U_G of (i) 1, (ii) 5, (iii) 10 and (iv) 30 cm.s^{-1}	45

2.19	Effect of characteristic time scale (i) $\tau = 0.05$ s and (ii) $\tau = 0.5$ s on instantaneous gas volume fraction fluctuations for U_G of (a) 1 and (b) 30 cm.s^{-1} ($X = 10$ cm, $Y = 76.5$ cm, $Z = 2.5$ cm).	46
2.20	(a) Effect of characteristic time scale ($\tau = 0.05, 0.5$ and 5.0 s) on instantaneous gas volume fraction fluctuations for U_G of 30 cm.s^{-1} ($X = 10$ cm, $Y = 76.5$ cm, $Z = 2.5$ cm) and (b) the variance for instantaneous gas volume fraction fluctuation time series calculated using different time scales (at $U_G = 1$ and 30 cm.s^{-1} , $X = 10$ cm, $Y = 76.5$ cm, $Z = 2.5$ cm).	48
2.21	Effect of characteristic time scale (i) $\tau = 0.05$ s and (ii) $\tau = 0.5$ s on frequency distribution for U_G of (a) 1 and (b) 30 cm.s^{-1} ($X = 10$ cm, $Y = 76.5$ cm, $Z = 2.5$ cm).	49
2.22	Effect of U_G on time-evolution of α_G fluctuations ($\tau = 0.5$ s, $X = 10$ cm, $Y = 76.5$ cm, $Z = 2.5$ cm) for U_G of (a) 1, (b) 5, (c) 10 and (d) 30 cm.s^{-1}	50
2.23	Effect of U_G on frequency distribution of gas-liquid flow (a) 1, (b) 5, (c) 10 and (d) 30 cm.s^{-1} ($\tau = 0.05$ s, $X = 10$ cm, $Y = 76.5$ cm, $Z = 2.5$ cm).	51
2.24	Bubble chord length distribution at $X = 1, 5$ and 10 cm for U_G of (a) 1, (b) 5, (c) 10 and (d) 30 cm.s^{-1} ($Y = 76.5$ cm, $Z = 2.5$ cm).	53
2.25	Number fraction distribution of bubbles with different chord lengths for U_G of (a) 1 and (b) 30 cm.s^{-1} ($X = 10$ cm, $Y = 76.5$ cm, $Z = 2.5$ cm). Enlarged view of classification of bubble population into different size groups is shown in the inset.	54
2.26	Bubble size distribution for U_G of 1 and 30 cm.s^{-1} ($X = 10$ cm, $Y = 76.5$ cm, $Z = 2.5$ cm).	55

2.27	Bubble size distribution at $X = 1, 5$ and 10 cm for U_G of (a) 1 , (b) 5 , (c) 10 and (d) 30 cm.s^{-1} ($Y = 76.5$ cm, $Z = 2.5$ cm).	56
2.28	Effect of U_G ($1 - 30 \text{ cm.s}^{-1}$) on bubble size distribution at three different heights (a) $Y = 9.7$ cm, (b) $Y = 27$ cm and (c) $Y = 76.5$ cm ($X = 10$ cm, $Z = 2.5$ cm).	57
2.29	Spatial distribution of time-averaged gas volume fraction for U_G in the range of $1 - 30 \text{ cm.s}^{-1}$, at two different heights (a) $Y = 27$ cm and (b) $Y = 76.5$ cm (at $Z = 2.5$ cm).	59
2.30	Number fraction distribution of gas phase points per bubble peak for U_G of (a) 1 , and (b) 30 cm.s^{-1} ($X = 10$ cm, $Y = 76.5$ cm, $Z = 2.5$ cm). Enlarged view and classification of bubble population into different size groups is shown in the inset.	60
2.31	Spatial distribution of time-averaged gas volume fraction decomposed according to bubble size groups for U_G of (a) 1 , (b) 5 , (c) 10 and (d) 30 cm.s^{-1} ($Y = 27$ cm, $Z = 2.5$ cm).	61
2.32	Spatial distribution of time-averaged gas volume fraction decomposed according to bubble size groups for U_G of (a) 1 , (b) 5 , (c) 10 and (d) 30 cm.s^{-1} ($Y = 76.5$ cm, $Z = 2.5$ cm).	62
3.1	(a) Schematic of a rectangular slurry bubble column and (b) Photograph of an in-house developed dual-tip voidage probe.	74
3.2	(a) Typical voltage signal acquired by a voidage probe, (b) normalized phase discriminated signal and (c) typical distribution of time interval and corresponding number of points in gas phase for which a probe tip remain in contact with bubbles.	75

3.3	Snapshots of gas–liquid–solid flow in a slurry bubble column for different solid loadings ($\langle \alpha_S \rangle = 0 - 40$ vol.%) at U_G of (a) 5 cm.s^{-1} and (b) 10 cm.s^{-1} and (c) 30 cm.s^{-1}	77
3.4	Instantaneous α_G fluctuations measured at $U_G = 5 \text{ cm.s}^{-1}$ for different solid loading of (a) 0, (b) 5 and (c) 20 vol.% ($\tau = 0.5$ s, $X = 10$ cm, $Y = 76.5$ cm, $Z = 2.5$ cm).	79
3.5	Instantaneous α_G fluctuations measured at $U_G = 30 \text{ cm.s}^{-1}$ for different solid loading of (a) 0, (b) 5 and (c) 40 vol.% ($\tau = 0.5$ s, $X = 10$ cm, $Y = 76.5$ cm, $Z = 2.5$ cm).	80
3.6	Time series of α_G fluctuations measured at three different lateral positions ($X = 1, 6$ and 10 cm) for solid loading of (a) 0 and (b) 20 vol.% ($U_G = 5 \text{ cm.s}^{-1}$, $\tau = 0.5$ s, $Y = 76.5$ cm, $Z = 2.5$ cm).	82
3.7	Time series of α_G fluctuations measured at three different lateral positions ($X = 1, 6$ and 10 cm) for solid loading of (a) 0 and (b) 20 and (c) 40 vol.% ($U_G = 30 \text{ cm.s}^{-1}$, $\tau = 0.5$ s, $Y = 76.5$ cm, $Z = 2.5$ cm).	83
3.8	Lateral evolution of the variance of α_G fluctuations (calculated using $\tau = 0.05$ s) for U_G of (a) 5 and (b) 30 cm.s^{-1} for various solid loadings (0-40 vol.%) ($Y = 76.5$ cm, $Z = 2.5$ cm).	85
3.9	Power spectra for α_G fluctuations in SBCR for solid loading of (a) 0, (b) 5, (c) 10 and (d) 20 vol.%, ($U_G = 5 \text{ cm.s}^{-1}$, $\tau = 0.05$ s, $X = 10$ cm, $Y = 76.5$ cm, $Z = 2.5$ cm).	86
3.10	Power spectra for α_G fluctuations in SBCR for solid loading of (a) 0, (b) 10, (c) 20 and (d) 40 vol.%, ($U_G = 30 \text{ cm.s}^{-1}$, $\tau = 0.05$ s, $X = 10$ cm, $Y = 76.5$ cm, $Z = 2.5$ cm).	87

3.11	Effect of solid loading (0-20 vol.%) on bubble chord length distribution in SBCR at U_G of (a) 5, (b) 10 and (c) 30 $cm.s^{-1}$ ($X = 10$ cm, $Y = 76.5$ cm, $Z = 2.5$ cm).	89
3.12	Number fraction of bubble chord lengths distributed in different size groups at U_G of (a) 5 and (b) 30 $cm.s^{-1}$ for different solid loadings (0-20 vol.%) ($X = 10$ cm, $Y = 76.5$ cm, $Z = 2.5$ cm). Enlarged view of classification of bubble population into different size groups for different solid loadings is shown in the inset.	90
3.13	Effect of solid loading (0-20 vol.%) on bubble size distribution for U_G of (i) 5, (ii) 10 and (iii) 30 $cm.s^{-1}$ at the liquid height of (a) $Y = 27$ cm and (b) $Y = 76.5$ cm ($X = 10$ cm, $Z = 2.5$ cm).	92
3.14	Effect of solid loading (0 - 20 vol.%) on lateral distribution of total (single-class) time-averaged gas volume fraction for U_G of (i) 5, (ii) 10 and (iii) 30 $cm.s^{-1}$ at the liquid height of (a) $Y = 27$ cm and (b) $Y = 76.5$ cm.	95
3.15	Effect of solid loading (0 - 20 vol.%) on lateral distribution of time-averaged gas volume fraction decomposed based on different bubble size groups (a) G_1 ($0 < y \leq 1.0$ cm), (b) G_2 (1.0 cm $< y \leq 2.0$ cm), (c) G_3 (2.0 cm $< y \leq 4.0$ cm) and (d) G_4 ($y > 4.0$ cm) at $U_G = 5$ $cm.s^{-1}$ ($Y = 76.5$ cm, $Z = 2.5$ cm).	96

3.16	Effect of solid loading (0 - 20 vol.%) on lateral distribution of time-averaged gas volume fraction decomposed based on different bubble size groups (a) G_1 ($0 < y \leq 1.0$ cm), (b) G_2 (1.0 cm $< y \leq 2.0$ cm), (c) G_3 (2.0 cm $< y \leq 4.0$ cm) and (d) G_4 ($y > 4.0$ cm) at $U_G = 10$ $cm.s^{-1}$ ($Y = 76.5$ cm, $Z = 2.5$ cm).	97
3.17	Effect of solid loading (0 - 20 vol.%) on lateral distribution of time-averaged gas volume fraction decomposed based on different bubble size groups (a) G_1 ($0 < y \leq 1.0$ cm), (b) G_2 (1.0 cm $< y \leq 2.0$ cm), (c) G_3 (2.0 cm $< y \leq 4.0$ cm) and (d) G_4 ($y > 4.0$ cm) at $U_G = 30$ $cm.s^{-1}$ ($Y = 76.5$ cm, $Z = 2.5$ cm).	98
4.1	(a) Schematic of rectangular bubble column, (b) computational grid, and (c) different sparger configurations with (i) 2.4 cm \times 1.2 cm inlet area (24 cells), (ii) single inlet hole/cell, and (iii) eight injection holes/cells.	113
4.2	Instantaneous snapshots of meandering bubble plume at U_G of (a) 0.16 $cm.s^{-1}$ and (b) 0.73 $cm.s^{-1}$, (i) experiments, (ii) simulated bubble concentration distribution (maximum concentration corresponds to 0.05 $kg.m^{-3}$ (red)), (iii) instantaneous bubble positions (colored by its rise velocity, maximum velocity corresponds to 1.0 $m.s^{-1}$ (red)), (iv) instantaneous liquid velocity flow field (maximum velocity corresponds to 0.5 $m.s^{-1}$ (red)).	115

4.3	Simulated snapshots of (i) instantaneous gas volume fraction and (ii) bubbles (colored by diameter = 0.5 cm) and (iii) liquid velocity (Y-component) distribution obtained using different sparger configurations, (a) 2.4 cm × 1.2 cm cross-section area (24 cells), (b) eight holes/cells and (c) single hole/cell, at $U_G = 0.73 \text{ cm.s}^{-1}$	117
4.4	Effect of mesh refinement on the time-averaged gas volume fraction profiles for $U_G = 0.73 \text{ cm.s}^{-1}$ at the liquid height of (a) 26.6 cm and (b) 76.8 cm ($Z = 2.5 \text{ cm}$)	119
4.5	Simulated ($\Delta t = 0.01 \text{ s}$) vs. measured ($\tau = 0.5 \text{ s}$) instantaneous gas volume fraction fluctuations at U_G of (a) 0.16 cm.s^{-1} and (b) 0.73 cm.s^{-1} ($X = 10 \text{ cm}$, $Y = 76.8 \text{ cm}$, $Z = 2.5 \text{ cm}$)	120
4.6	Simulated instantaneous liquid velocity distribution with and without size-dependent lift force (\vec{F}_L) for mono-dispersed bubble flow ($d_B = 0.5 \text{ cm}$) at (a) $U_G = 0.16 \text{ cm.s}^{-1}$ and (b) $U_G = 0.73 \text{ cm.s}^{-1}$ ($X = 10 \text{ cm}$, $Y = 76.8 \text{ cm}$, $Z = 2.5 \text{ cm}$)	122
4.7	(i) Simulated snapshots and (ii) corresponding instantaneous α_G time series (with \vec{F}_D and \vec{F}_L) for mono-dispersed bubbles of size, (a) 0.1 cm, (b) 0.5 cm, and (c) 1.0 cm at $U_G = 0.73 \text{ cm.s}^{-1}$ ($X = 10 \text{ cm}$, $Y = 76.8 \text{ cm}$, $Z = 2.5 \text{ cm}$)	124
4.8	Simulated instantaneous liquid velocity time series for mono-dispersed bubbly flow of ($d_B = 0.1, 0.5$ and 1.0 cm) with (a) \vec{F}_D only and (b) $\vec{F}_D + \vec{F}_L$ at $U_G = 0.73 \text{ cm.s}^{-1}$ ($X = 10 \text{ cm}$, $Y = 76.8 \text{ cm}$, $Z = 2.5 \text{ cm}$) . . .	126

4.9	Predicted (with inclusion of different combinations of \vec{F}_D and \vec{F}_L) and measured time-averaged gas volume fraction profiles for (a) $U_G = 0.16 \text{ cm.s}^{-1}$ and (b) $U_G = 0.73 \text{ cm.s}^{-1}$ at the liquid heights of (i) $Y = 26.6 \text{ cm}$ and (ii) $Y = 76.8 \text{ cm}$ ($Z = 2.5 \text{ cm}$)	127
4.10	Predicted (with inclusion of different combinations of \vec{F}_D and \vec{F}_L) time-averaged axial liquid velocity profiles for (a) $U_G = 0.16 \text{ cm.s}^{-1}$ and (b) $U_G = 0.73 \text{ cm.s}^{-1}$ ($Y = 76.8 \text{ cm}$, $Z = 2.5 \text{ cm}$)	129
4.11	Predicted (with inclusion of different combinations of \vec{F}_D and \vec{F}_L) and measured bubble rise velocity distribution for (a) $U_G = 0.16 \text{ cm.s}^{-1}$ and (b) $U_G = 0.73 \text{ cm.s}^{-1}$ at the liquid height of $Y = 50 \text{ cm}$	130
4.12	Instantaneous gas/bubble distribution at (a) $U_G = 0.16 \text{ cm.s}^{-1}$ and (b) $U_G = 0.73 \text{ cm.s}^{-1}$, (i) experiments, (ii) mono-dispersed bubble flow ($d_B = 0.5 \text{ cm}$) without lift force, (iii) mono-dispersed bubble flow ($d_B = 0.5 \text{ cm}$) with lift force, (iv) poly-dispersed bubble flow ($d_B = 0.1, 0.5$ and 1.0 cm) without lift, (v) poly-dispersed bubble flow ($d_B = 0.1, 0.5$ and 1.0 cm) with lift force (Bubbles are colored according to their diameters i.e. 0.1 cm (blue); 0.5 cm (green); 1.0 cm (red))	133
5.1	(a) Boundary conditions, (b) side wall and (c) 3D grid for the rectangular bubble column.	146
5.2	Gas-liquid flow in a rectangular BCR (a) experimental snapshot and (b) simulated instantaneous gas volume fraction distribution at U_G of (i) 1, (ii) 5, (iii) 10, (iv) 20, and (v) 30 cm.s^{-1}	148
5.3	Simulated instantaneous liquid velocity distribution at U_G of (i) 1, (ii) 5, (iii) 10, (iv) 20, and (v) 30 cm.s^{-1}	149

5.4	Effect of mesh refinement on time-averaged gas volume fraction profiles for U_G of (a) 5 and (b) 10 cm.s^{-1} at the liquid height (i) $Y = 27$ cm and (ii) $Y = 76.5$ cm ($Z = 2.5$ cm).	150
5.5	Predicted vs. measured overall gas volume fraction for U_G in the range of 1 - 30 cm.s^{-1} using different drag correction factor ($C_D = C_{D_0} (1 - \alpha_G)^p$ where $p = 0, 2,$ and 4).	152
5.6	Effect of drag correction factor ($p = 0$ and 2) on time-averaged gas volume fraction profile for $U_G = 10$ cm.s^{-1} at the liquid heights of (a) $Y = 27$ cm and (b) $Y = 76.5$ cm ($Z = 2.5$ cm).	153
5.7	Simulated ($\Delta t = 0.01$ s) vrs. measured ($\tau = 0.01$ s) instantaneous gas volume fraction fluctuations at U_G of (a) 1, (b) 5, (c) 10, and (d) 30 cm.s^{-1} ($X = 10$ cm, $Y = 76.5$ cm, $Z = 2.5$ cm).	155
5.8	Variance (σ) calculated from instantaneous α_G time-series for U_G in the range of 1-30 cm.s^{-1} ($X = 10$ cm, $Y = 76.5$ cm and $Z = 2.5$ cm).	157
5.9	(a) Measured ($\tau = 0.01$ s) and (b) simulated ($\Delta t = 0.01$ s) power spectral density distribution at U_G of (i) 1, (ii) 5, (iii) 10 and (iv) 30 cm.s^{-1} ($X = 10$ cm, $Y = 76.5$ cm and $Z = 2.5$ cm).	158
5.10	(a) Time-evolution of instantaneous α_G and (b) power spectral density obtained from experiments at 30 cm.s^{-1} using τ of (i) 0.01 s, (ii) 0.05 s and (iii) 0.5 s, and simulations using $\Delta t = 0.01$ s ($X = 10$ cm, $Y = 76.5$ cm and $Z = 2.5$ cm).	159
5.11	Comparison of PSD obtained from α_G fluctuations measured using $\tau = 0.5$ s and predicted using $\Delta t = 0.01$ s at U_G of (i) 1, (ii) 5, (iii) 10 and (iv) 30 cm.s^{-1} ($X = 10$ cm, $Y = 76.5$ cm and $Z = 2.5$ cm).	160

5.12	Comparison of predicted and measured time-averaged gas volume fraction profiles at U_G of 1-30 cm.s^{-1} at the axial locations of (a) $Y = 27$ cm and (b) $Y = 76.5$ cm ($Z = 2.5$ cm).	161
5.13	Effect of U_G (1 - 30 cm.s^{-1}) on predicted time-averaged liquid velocity distribution at axial locations of (a) $Y = 27$ cm (b) $Y = 76.5$ cm ($Z = 2.5$ cm).	162
5.14	Comparison of predicted vs. measured time-averaged gas volume fraction profiles near wall region at U_G of 10 cm.s^{-1} ($Y = 76.5$ cm and $Z = 2.5$ cm).	164
6.1	Effect of $\langle \alpha_S \rangle$ on experimental and simulated flow behavior of gas–liquid–solid flows at U_G of (a) 5, (b) 10 and (c) 30 cm.s^{-1} on (i) experiments, (ii) simulated instantaneous gas volume fraction (0 (blue) to 0.3 (red)) and (iii) simulated instantaneous solid volume fraction (0 (blue) to 0.15 (red)).	180
6.2	Snapshots of simulated instantaneous axial liquid velocity (different volume % of solids) in a SBCR at U_G of (a) 5 and (b) 30 cm.s^{-1} .	181
6.3	Instantaneous gas volume fraction at four different solid loadings, (a) 0, (b) 5, (c) 10 and (d) 20 v/v % at $U_G = 5$ cm.s^{-1} ($X = 10$ cm, $Y = 76.5$ cm, $Z = 2.5$ cm).	182
6.4	Instantaneous gas volume fraction at four different solid loadings, (a) 0, (b) 5, and (c) 20 v/v % at $U_G = 10$ cm.s^{-1} ($X = 10$ cm, $Y = 76.5$ cm, $Z = 2.5$ cm).	183
6.5	Instantaneous gas volume fraction at four different solid loadings, (a) 0, (b) 5, and (c) 20 v/v % at $U_G = 30$ cm.s^{-1} ($X = 10$ cm, $Y = 76.5$ cm, $Z = 2.5$ cm).	184

6.6	The variance (σ) corresponding to the instantaneous α_G fluctuations using simulations ($\Delta t = 0.01$ s) and measurements ($\tau = 0.01$ and 0.5 s) for $\langle \alpha_S \rangle$ of (a) 0, (b) 5, (c) 10 and (d) 20 v/v% for U_G in the range of $5-30 \text{ cm.s}^{-1}$ ($X = 10$ cm, $Y = 76.5$ cm, $Z = 2.5$ cm).	186
6.7	Comparison of predicted and measured power spectra corresponding to the α_G fluctuations obtained from (a) experiments ($\tau = 0.01$ s) and (b) simulations ($\Delta t = 0.01$ s) for solid loading, (i) 0, (ii) 5, (iii) 10 and (iv) 20 v/v % at $U_G = 5 \text{ cm.s}^{-1}$ ($X = 10$ cm, $Y = 76.5$ cm, $Z = 2.5$ cm). . . .	187
6.8	Comparison of predicted and measured power spectra corresponding to the α_G fluctuations obtained from (a) experiments ($\tau = 0.01$ s) and (b) simulations ($\Delta t = 0.01$ s) for solid loading, (i) 0, (ii) 5, (iii) 20 and (iv) 40 v/v % at $U_G = 30 \text{ cm.s}^{-1}$ ($X = 10$ cm, $Y = 76.5$ cm, $Z = 2.5$ cm). . . .	188
6.9	Predicted vs. measured overall gas volume fraction in SBCR.	190
6.10	Measured vs. predicted time-averaged gas volume fraction at different solid loading (0-20 v/v %) at liquid heights (a) $Y = 27$ cm and (b) $Y = 76.5$ cm ($Z = 2.5$ cm) at $U_G = 5 \text{ cm.s}^{-1}$	191
6.11	Measured vs. predicted time-averaged gas volume fraction at different solid loading (0-20 v/v %) at liquid heights (a) $Y = 27$ cm and (b) $Y = 76.5$ cm ($Z = 2.5$ cm) at $U_G = 10 \text{ cm.s}^{-1}$	192
6.12	Measured vs. predicted time-averaged gas volume fraction at different solid loading (0-20 v/v %) at liquid heights (a) $Y = 27$ cm and (b) $Y = 76.5$ cm ($Z = 2.5$ cm) at $U_G = 30 \text{ cm.s}^{-1}$	193

6.13 Predicted lateral distribution of time-averaged axial liquid velocity (Y-
component) at different solid loading (0-20 v/v%) and U_G of (a) 5 and
(b) 30 cm.s^{-1} (Y = 76.5 cm and Z = 2.5 cm). 196

List of Tables

5.1	Physical properties and model parameters used for the simulations . . .	145
6.1	Summary of the experimental conditions* used in this work	178